On the T-stress and its influence on the constraint due to specimen thickness and crack length under mode-I loading

A. Fernández-Canteli[1], *J. Fernández Sáez*[2], *D. Fernández Zúñiga*[1]
[1]*EPSIG, University of Oviedo, Gijón, Spain;*
[2]*University Carlos III, Leganés, Madrid, Spain*

Abstract

A novel approach, based on the tensor character of the stress intensity at the crack front, is presented with the aim of correlating the influence of typical in- and out-of-plane constraint cases to the apparent fracture toughness of materials under mode-I loading in the scope of the LEFM. The analysis demonstrates the invariability of the stress intensity tensor k_{ij} at the crack front, irrespective of the specimen thickness, and the necessity of considering, additionally, the constraint tensor t_{ij}, corresponding to the second constant term in Williams expansion to explain the different fracture toughnesses resulting from the loss of constraint. Both components of t_{ij}, the t_{xx}, or conventional *T*-stress, and the out-of-plane component t_{zz} are evaluated under different constraint conditions showing, in general, higher values for t_{zz} than for t_{xx}, notably for $B < B_{\min}$. The approach proposed represents an extension of the current biparametric approach, based on the T-stress that proves to be only capable to cope with in-plane constraint cases.

1. INTRODUCTION

The increase in the apparent fracture toughness due to the loss of constraint has been recognized in a number of experimental programs (see [1-3]) having an important repercussion in practical situations, in which the consideration of a enhancement in the fracture toughness may contribute to economize the design of brittle elements in the presence of cracks according to the LEFM. The biparametric approaches based on the *T*-stress, allows for in-plane constraint effects, such as those arising from crack length influence, but fails to cope with those related to out-of-plane constraint, as is the case with the specimen thickness. In fact, the influence of the latter is noticeable when $B < B_{\min}$ leading to a considerable rise in the apparent fracture toughness, even for moderate reductions of the specimen thickness, without the *T*-stress being influenced. This suggests questioning the pertinence of considering the *T*-stress as the only reference parameter to explain general loss of constraint effects and to search for new, more general, solutions.

In this work, an approach is developed within the scope of the LEFM, based on new defined magnitudes derived from the three-dimensional stress and strain

tensor field at the crack front. These are the stress intensity tensor k_{ij} and the constraint tensor t_{ij} from Williams expansion, and the constraint functions ψ_{ij} (see [4,5]). Analytical relations are found, and numerical calculations performed allowing us to investigate the influence of both the specimen thickness *B*, using Arcan Richard (in what follows A-R) specimens, and the crack length *a/W*, using SENB specimens, on the constraint tensor t_{ij} by comparing the values of the in-plane component t_{xx}, i.e., the T-stress, with those of the out-of-plane component t_{zz} for different loss of constraint relations. This model represents an extension of the current biparametric approach, and proves to be adequate to tackle both in- and out-of plane kinds of constraint that should be subsequently considered in establishing the fracture criterion

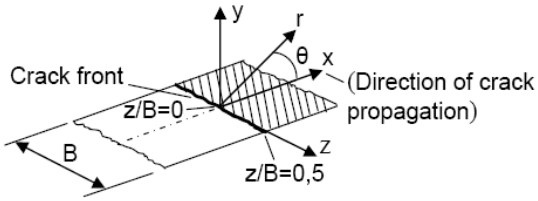

Fig.1: Crack front and associated coordinate systems (cartesian and polar).

2. STRESS AND STRAIN RELATIONS AT THE CRACK FRONT

Let us consider a linear elastic solid containing a through-thickness crack subjected to mode I loading. The following new tensor magnitudes are defined for a given specimen thickness *B*:

a) stress intensity field tensor or half moment stress tensor, as

$$\phi_{ij}(z,r,\theta;B)=\sqrt{2\pi r}\;\sigma_{ij}(z,r,\theta;B)\ , \tag{1}$$

b) directional stress intensity tensor as:

$$h_{ij}(z,\theta;B)==\lim_{r\to 0}\phi_{ij}(z,r,\theta;B)=\lim_{r\to 0}\sqrt{2\pi r}\;\sigma_{ij}(z,r,\theta;B)\ , \tag{2}$$

c) stress intensity tensor as:

$$k_{ij}(z;B)=h_{ij}(z,\theta;B)\Big|_{\theta=\theta_{cr}}=\lim_{r\to 0}\sqrt{2\pi r}\;\sigma_{ij}(z,r,\theta;B)\ \Big|_{\theta=\theta_{cr}}\ , \tag{3}$$

where, *r* is the distance to the crack front, *z* is the location at the crack front and θ is the orientation angle considered. Assuming validity of the Williams expansion [6], also for the out-of-plane component σ_{zz}, the stress tensor in the proximity of the crack front may be expressed as:

$$\sigma_{ij}(z,r,\theta;B)=\frac{h_{ij}(z,\theta;B)}{\sqrt{2\pi r}}+t_{ij}(z;B)+0(r^{1/2};B)\ , \tag{4}$$

in which $h_{ij}(z,\theta;B)$ is given by (2), $t_{ij}(z;B)$ is the θ independent constant stress tensor and $0(r^{1/2};B)$ represents generically the remaining higher order terms.

With reference to the system showed in Figure 1 under mode-I loading, it follows that

$$h_{xx}(z,\theta;B) = k_{xx}(z;B) f_{xx}(\theta) = k_{xx}(z;B)[\cos\frac{\theta}{2}(1-\sin\frac{\theta}{2}\sin\frac{3\theta}{2})]$$
$$h_{yy}(z,\theta;B) = k_{yy}(z;B) f_{yy}(\theta) = k_{xx}(z;B)[\cos\frac{\theta}{2}(1+\sin\frac{\theta}{2}\sin\frac{3\theta}{2})] \quad (5)$$
$$h_{zz}(z,\theta;B) = k_{zz}(z;B) f_{zz}(\theta) = k_{zz}(z;B)\cos\frac{\theta}{2},$$

where $f_{ij}(\theta)$ are the angular functions associated with the first term of Williams expansion, here extended to three-dimensional case (see [5-7]). Applying the generalized Hooke's law, the out-of-plane strain $\varepsilon_{zz}(z,r,\theta;B)$ in the proximity of the crack front results, after rearranging terms, in

$$\varepsilon_{zz}(r,\theta) = \frac{1}{E}\left[\frac{h_{zz}(z,\theta;B) - \nu\,(h_{xx}(z,\theta;B) + h_{yy}(z,\theta;B))}{\sqrt{2\pi r}} + t_{zz}(z;B) - \nu\,(t_{xx}(z;B) + t_{yy}(z;B) + 0\,(r^{1/2};B)\right], \quad (6)$$

where ν is the Poisson coefficient of the material. Since the out-of-plane displacement at a generic position *z* of the crack front $u_z(z,0,\theta;B)$, given by

$$u\ (z,0,\theta;B) = \int_0^z \varepsilon_{zz}(z,0,\theta;B)\,dz\,, \quad (7)$$

must be bounded, the out-of-plane strain $\varepsilon_{zz}(z,r,\theta;B)$ at $r=0$ cannot be singular. Allowing for (6), this requires the condition

$$h_{zz}(z,\theta;B) - \nu\,[h_{xx}(z,\theta;B) + h_{yy}(z,\theta;B)] = 0\,. \quad (8)$$

Replacing (5) into (8) gives:

$$k_{zz}(z;B) f_{zz}(\theta) - \nu\,[k_{xx}(z;B) f_{xx}(\theta) + k_{yy}(z;B) f_{yy}(\theta)] = 0\,. \quad (9)$$

For mode-I loading, $\theta = \theta_{cr} = 0^{\circ}$, and $f_{xx}(\theta_{cr}) = f_{yy}(\theta_{cr}) = f_{zz}(\theta_{cr}) = 1$, so that Expr. (9) transforms into

$$k_{zz}(z;B) - \nu\,[k_{xx}(z;B) + k_{yy}(z;B)] = 0\,, \quad (10)$$

proving that the stress intensity tensor $k_{ij}(z;B)$ results, invariably, given in the form

$$k_{ij}(z;B) = \begin{pmatrix} K_I(z;B) & 0 & 0 \\ 0 & K_I(z;B) & 0 \\ 0 & 0 & 2\nu K_I(z;B) \end{pmatrix} = K_I(z;B) \begin{pmatrix} 1 & 0 & 0 \\ 0 & 1 & 0 \\ 0 & 0 & 2\nu \end{pmatrix}, \quad (11)$$

irrespective of the specimen thickness. This demonstrates the independence of the structure of the stress intensity tensor $k_{ij}(z;B)$ with respect to the constraint level for given in-plane stress intensity factor $K_I(z;B)$.

3. THE TENSOR t_{ij} AS A MEASURE OF CONSTRAINT

At the crack front *r=0*, the singular term as well as the $r^{1/2}$ and higher terms of Williams expansion of the out-of-plane strain ε_{zz} vanish for any *B*, so that (see (6)).

$$\varepsilon_{zz}(z,r;B)\big|_{r=0} = \lim_{r\to 0}\frac{\sigma_{zz}(z,r;B)-\nu\,(\sigma_{xx}(z,r;B)-\sigma_{yy}(z,r;B))}{E} = \frac{t_{zz}(z;B)-\nu\,t_{xx}(z;B)}{E}. \quad (12)$$

Due to the symmetry, the tensor $t_{ij}(z,B)$ for mode-I loading at the mid-plane of the specimen is given by

$$t_{ij}(0;B)=\begin{pmatrix} t_{xx}(0;B) & 0 & 0 \\ 0 & 0 & 0 \\ 0 & 0 & t_{zz}(0;B) \end{pmatrix}=\begin{pmatrix} t_{xx}(0;B) & 0 & 0 \\ 0 & 0 & 0 \\ 0 & 0 & E\varepsilon_{zz}(0;B)+\nu t_{xx}(0;B) \end{pmatrix}. \quad (13)$$

For $B\to\infty$, identified as a plane strain case, ε_{zz} may be neglected. Then (12) reduces to $t_{zz}(z;B)\cong\nu\,t_{xx}$ and (13) becomes

$$\lim_{B\to\infty} t_{ij}(0;B)=\begin{pmatrix} \lim_{B\to\infty} t_{xx}(0;B) & 0 & 0 \\ 0 & 0 & 0 \\ 0 & 0 & \nu\lim_{B\to\infty} t_{xx}(0;B) \end{pmatrix}=\lim_{B\to\infty} t_{xx}(0;B)\begin{pmatrix} 1 & 0 & 0 \\ 0 & 0 & 0 \\ 0 & 0 & \nu \end{pmatrix}=T(0)\begin{pmatrix} 1 & 0 & 0 \\ 0 & 0 & 0 \\ 0 & 0 & \nu \end{pmatrix} \quad (14)$$

proving that in such a case, the tensor $t_{ij}(z;B)$ turns out to be a linear function of the $t_{xx}(0;B\to\infty)$ component, and can be properly supplanted by the conventional *T*-stress as suggested by the current biparametric approach. However, in the case of a specimen of real thickness $0<B<\infty$, notably for $B<B_{\min}$, where $B_{\min}$ is the minimum specimen thickness, Expr. (13) rather than (14) is the only correct expression to represent the constraint influence on the apparent fracture toughness for a specimen thickness *B*.

4. DERIVATION OF t_{xx} AND t_{zz} FROM THE STRESS FIELD

Different procedures have been applied to calculate the T-stress, as for instance that suggested in [8], according to which the t_{xx} value is found as

$$t_{xx}(B)=\lim_{r\to 0}\tau_{xx}(r,\theta;B)\ , \quad (15)$$

where τ_{xx} is a function of the stresses given by

$$\tau_{xx}(r,\theta;B)=\sigma_{xx}(r,\theta;B)+\alpha\,\sigma_{yy}(r,\theta;B)\ , \quad (16)$$

and α results from the condition

$$\alpha = -\frac{f_{xx}(\theta)}{f_{yy}(\theta)} = -\frac{\cos\frac{\theta}{2}(1-\sin\frac{\theta}{2}\sin\frac{3\theta}{2})}{\cos\frac{\theta}{2}(1+\sin\frac{\theta}{2}\sin\frac{3\theta}{2})} = -\frac{1-\sin\frac{\theta}{2}\sin\frac{3\theta}{2}}{1+\sin\frac{\theta}{2}\sin\frac{3\theta}{2}} \ , \tag{17}$$

aiming to avoid the presence of the S.I.F. K_I in the derivation. f_{xx} and f_{yy} are the angular functions related to the singular term in Williams expansion. This allows us to derive t_{xx}, i.e., the *T*-stress, as a function of the orientation angle θ.

Applying a similar procedure for t_{zz} leads to

$$t_{zz}(B) = \lim_{r\to 0} \tau_{zz}(r,\theta;B) \ , \tag{18}$$

where τ_{zz} is a function of the stresses given by

$$\tau_{zz}(r,\theta;B) = \sigma_{zz}(r,\theta;B) + \beta\, 2\nu\, \sigma_{yy}(r,\theta;B) \, , \tag{19}$$

and

$$\beta = -\frac{2\nu\, f_{zz}(\theta)}{f_{yy}(\theta)} = -\frac{2\nu\cos\frac{\theta}{2}}{\cos\frac{\theta}{2}(1+\sin\frac{\theta}{2}\sin\frac{3\theta}{2})} = -\frac{2\nu}{1+\sin\frac{\theta}{2}\sin\frac{3\theta}{2}} \ . \tag{20}$$

This permits the stress t_{zz} to be found as a function of the orientation angle θ.

5. NUMERICAL ANALYSIS

With the aim of checking the validity of the preceding theoretical derivations and to investigate their possible practical applications, linear elastic three-dimensional numerical calculations were performed for aluminum alloy Al 7075 Arcan-Richard (A-R) and SENB specimens using the finite element ABAQUS code (see Fig. 2). The mechanical and fracture properties of the material used were: E=71000 MPa, ν=0.34, $R_{p0.2}$=533 MPa, K_{Ic}=30 MPam$^{1/2}$ and K_{IIc}=44.4 MPam$^{1/2}$, B_{min}=7.9 mm. The specimens were subjected to the critical load corresponding to the fracture toughness of the material. In the A-R specimens, a constant width W=50 mm provided with a crack length a/W=0.50 was assumed throughout the calculations.

A finite element mesh of the type shown in Fig. 2 was considered. It initiates with a 1 μm element size, which is steadily increased using a 1.22 size ratio allowing a detailed stress analysis in the region immediate to the crack front to be performed. The reason for selecting A-R non-standard specimens for the calculations is due to its further potential applications to mode-II or mixed-mode loading.

5.1 Constraint functions

The so-called constraint functions $\psi_{ij}(z,r;B)$ are defined as

$$\psi_{ij}(z,r;B) = \phi_{ij}(z,r,\theta_{cr};B) = \sqrt{2\pi r}\ \sigma_{ij}(z,r,\theta_{cr};B) \quad . \tag{21}$$

They represent the stress intensity field in the direction of the prospective crack propagation, i.e., $\theta = \theta_{cr} = 0°$ for mode-I loading, and supply relevant information on the three-dimensional near stress field allowing us to characterize the constraint at the crack front. Replacing the stress expressions in (4) for the critical direction for mode-I, $\theta = 0$, into (1) results in

$$\psi_{ij}(z,r;B) = k_{ij}(z;B) + \sqrt{2\pi r}\ t_{ij}(z;B) + 0\,(r^{1/2};B) \tag{22}$$

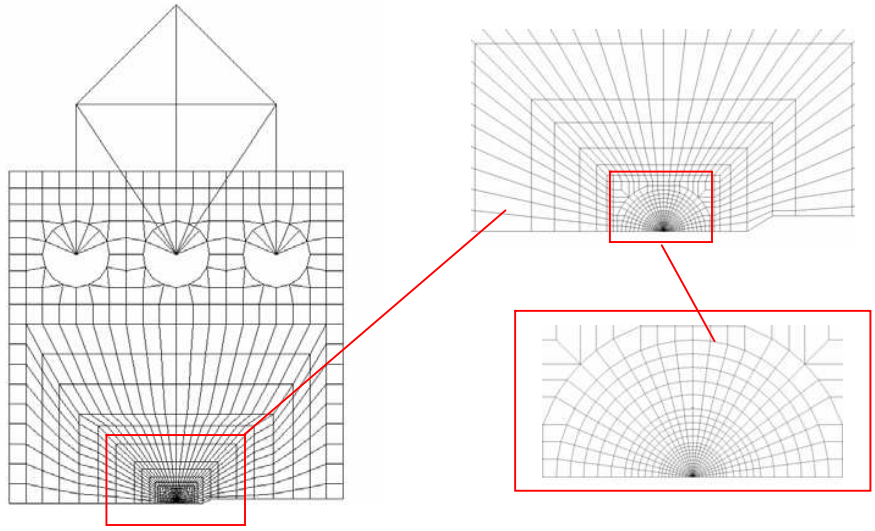

Fig. 2: Modeling the A-R specimen under mode-I loading and F.E. mesh.

At the crack front, i.e., for $r \to 0$ the constraint functions $\psi_{ij}(z,r;B)$ converge to the respective stress intensity tensor components $k_{ij}(z;B)$. Figure 3 shows the constraint functions $\psi_{ij}(0,r;B)$ along the *x*-axis at the mid-plane of A-R specimens for a wide range of specimen thicknesses (see [5]). Since, according to (11), the structure of the stress intensity tensor does not depend on the constraint, the convergence of the constraint functions to k_{ij} for $r \to 0$ is ensured independently of the constraint level. As a consequence, the shape of the different constraint functions $\psi_{xx}(z,r;B)$, $\psi_{yy}(z,r;B)$ or $\psi_{zz}(z,r;B)$ resulting for different specimen thicknesses may be attributed only to the influence of the respective components of the second and/or higher order terms of the Williams expansion. This is particularly noticeable by the out-of plane constraint function $\psi_{zz}(z,r;B)$, pointing

out the influence of the component t_{zz} of the tensor t_{ij} on the loss of constraint due to the thickness effect (see Figs. 3 and 4).

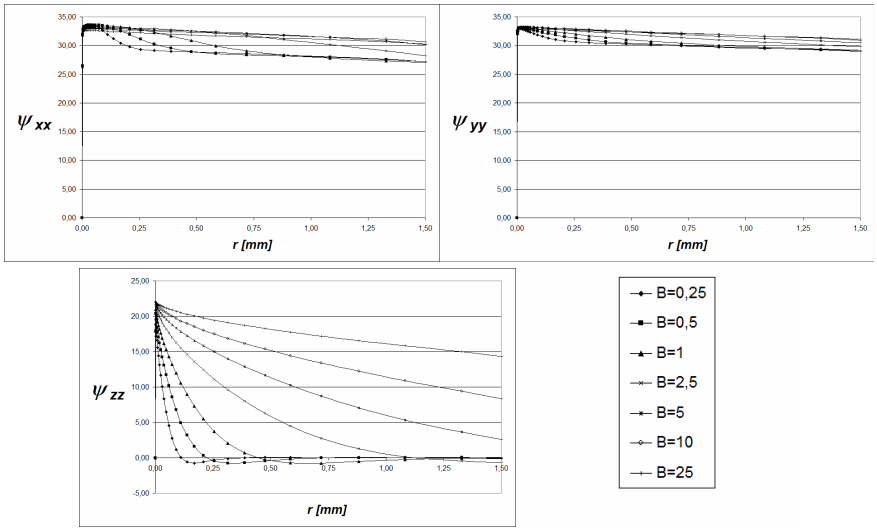

Fig. 3: Constraint functions $\psi_{ij}(z,r;B)$ at the mid-plane of A-R specimens under mode-I loading (from [5]).

The constraint function $\psi_{zz}(z,r;B)$ gets normalized, denoted $\overline{\psi}_{zz}(\overline{z},\overline{r})$, when dimensionless magnitudes, $\overline{\psi}_{zz} = \psi_{zz} / k_{zz} = \psi_{zz} / 2\nu K_I$, $\overline{z} = z / B$ and $\overline{r} = r / B$ are used (see Fig. 5). Note that a normalized t_{zz} may be directly derived from the $\overline{\psi}_{zz}(\overline{z},\overline{r})$ function, so that the t_{zz} value for whichever specimen thickness can be obtained using a unique FE calculation.

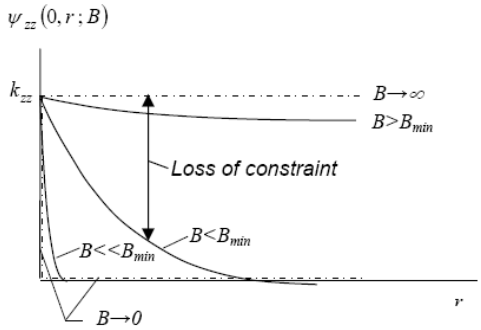

Fig. 4: Schematic representation of the out-of-plane constraint functions $\psi_{zz}(z,r;B)$ at the mid-plane of specimens for a variety of different thicknesses.

Table 1: Estimated t_{xx} and t_{zz} values at the mid-plane for A-R specimens with constant *a/W* ratio and different thickness *B*.

B[mm]	t_{xx}*[MPa]*	t_{zz}*[MPa]*	*B[mm]*	t_{xx}*[MPa]*	t_{zz}*[MPa]*
0.25	-9	-800	2.5	-9	-240
1	-9	-400	10	-9	-120

In the case of very thin specimens, the back-normalization of $\overline{\psi}_{zz}(\bar{z},\bar{r})$ for $B \to 0$ leads to a dimensional constraint function practically coinciding with the ordinate axis (see Figs. 3 and 4) while the initial point of the curve remains k_{zz}. This evidences the persistent singular nature of the out-of-plane stress σ_{zz} for $B \to 0$.

5.2 Calculation of t_{xx} and t_{zz} in a case of out-of-plane constraint

The effect of the specimen thickness on the constraint is investigated using A-R specimens for four different thicknesses. Table 1 gives the estimated values obtained at the mid-plane setting the stresses resulting from the FE calculations into Exprs. (15) and (16) for t_{xx} and (18) and (19) for t_{zz}. A strong dependence of the t_{xx} values has been observed with respect to the orientation considered impeding a reliable estimation of its value. A more reliable value has been found using 2-D FE calculation (see [9]) assuming no influence of the specimen thickness on the t_{xx} value under such conditions.

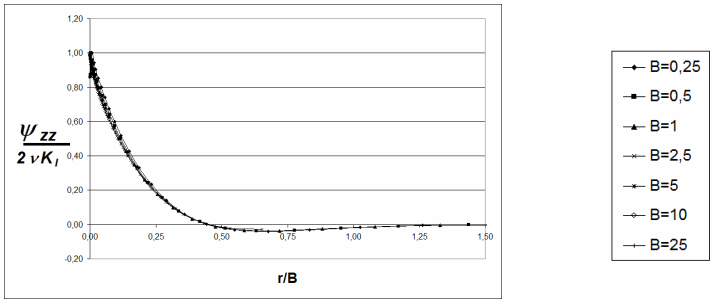

Fig. 5: Dimensionless constraint function $\overline{\psi}_{zz}(\bar{z},\bar{r})$ for A-R specimens under mode-I of loading (from [5]).

5.3 Calculation of t_{xx} and t_{zz} in a case of in-plane constraint

The effect of the crack size on the constraint has been also numerically investigated by means of finite elements calculations on 3-point bend (SENB) specimens with fixed dimensions, *H=100 mm, W=50 mm, s=200 mm*, first for variable crack length ratios *a/W* (0.05, 0.10, 0.20, 0.30, 0.40 and 0.50) and constant specimen thickness *B*=1 mm, denoted case 1, then for constant crack length ratio *a/W=0.10* and different thickness B (0.25, 1,00, 2.50 and 10 mm), denoted case 2. Thus a representative range of these parameters is covered including both negative and positive values of the t_{xx} component, i.e., the *T*-stress.

In the crack immediacy, the FE mesh for the SENB specimen coincides with that used for the A-R FE calculations. Outside this zone, the mesh tends to accommodate to the particular morphology of the SENB specimen.

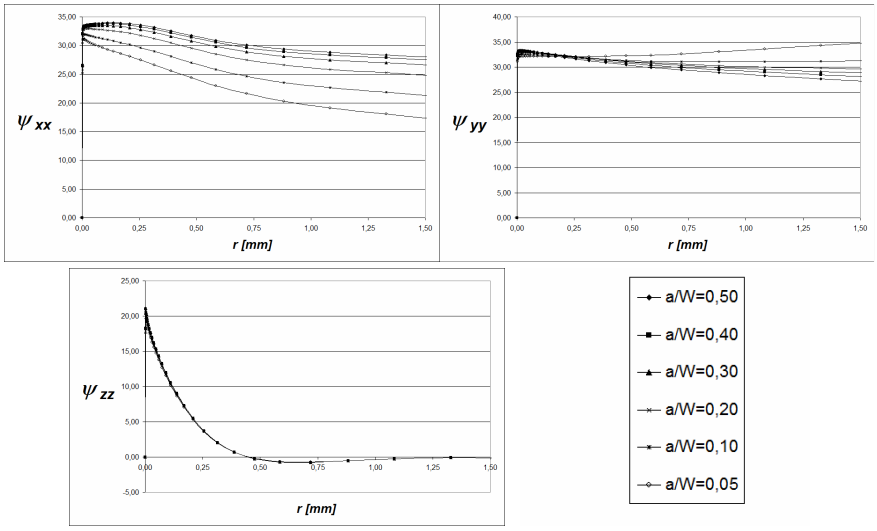

Fig. 6: Constraint functions ψ_{xx}, ψ_{yy} and ψ_{zz} for 3-point bend (SENB) specimens with different *a/W* ratios and constant thickness *B*=1 mm.

Tables 2 and 3 show the values of the t_{xx} and t_{zz} components estimated for case 1 and case 2, respectively, setting the stresses resulting from the FE calculations into Exprs. (15) and (16) for t_{xx} and (18) and (19) for t_{zz}.

Table 2: Estimated t_{xx} and t_{zz} values for 3-point bending SENB specimens with different *a/W* ratios and constant thickness *B*=1 mm.

a/W	t_{xx}*[MPa]*	t_{zz}*[MPa]*	*a/W*	t_{xx}*[MPa]*	t_{zz}*[MPa]*
0.05	-160	-400	0.30	-18	-400
0.10	-90	-400	0.40	-1	-400
0.20	-42	-400	0.50	+13	-400

Table 3: Estimated t_{xx} and t_{zz} values for 3-point bending SENB specimens with constant crack length ratio *a/W*= 0.10 and different specimen thickness *B*.

B[mm]	t_{xx}*[MPa]*	t_{zz}*[MPa]*	*B[mm]*	t_{xx}*[MPa]*	t_{zz}*[MPa]*
0.25	-90	-800	2.5	-90	-250
1	-90	-400	10	-90	-125

Again, the t_{xx} component becomes a small fraction of the t_{zz} component, even for the lowest *a/W* ratios, confirming the necessity of considering the whole tensor t_{ij} containing the t_{zz} component when establishing the instability criterion. In fact, according to (12) significant variations in the ε_{zz} values at the crack front are expected for the different *a/W* ratios, account given of the variability of the t_{xx} and constancy of t_{zz} the component, thus proving the absence of plane strain conditions at the crack front.

6. CONCLUSIONS

- The stress tensor σ_{ij} in the proximity of a crack can be obtained as a sum of infinite tensor series, based on Williams expansion.

- Alternatively, only two tensors can be used to describe, as an approximation, the stress state at the crack vicinity: the stress intensity tensor k_{ij} and the constraint tensor t_{ij}.

- Since the structure of the stress intensity tensor k_{ij} is invariable for any constraint state, the constraint tensor t_{ij}, becomes the discriminating tensor, hence indispensable to define the crack instability conditions under loss of constraint conditions.

- Consequently, the consideration of the T-stress, i.e., the t_{xx} component of the t_{ij} tensor, is insufficient to define the constraint in a real specimen, in which, necessarily, both in-plane and out-of-plane constraint phenomena are implied.

- The theoretical derivations developed in this paper justified those statements. The numerical calculations confirm the proposed approach using two types of specimens in which the constraint parameters are varied in a representative range.

7. BIBLIOGRAPHY

[1] J.M. Barson, S.T. Rolfe, Fracture and fatigue control in structures, 2nd Edition, Prentice Hall, Englewood Cliffs., 1987

[2] C. Betegón , F.J. Belzunce, C. Rodríguez, A two parameter fracture criterion for high strength low carbon steel, Acta Mater 44 (3) (1996), 1055-1061

[3] W. Hiese, Gültigkeitskriterien zur Bestimmung von Scherbruchzähigkeiten, Doctoral thesis, Ruhr-Universität Bochum, 2000

[4] D. Fernández-Zúñiga, J. Fernández-Sáez, A. Fernández-Canteli, On the T-stress and its relation with the loss of constraint (in Spanish), An Mec Frac 25 (2008) 522-529

[5] A. Fernández-Canteli, E. Castillo, D. Fernández-Zúñiga, Linear elastic fracture mechanics based criteria for fracture including out-of-plane constraint effect (2008) submitted to Strain

[6] M.L. Williams, On the stress distribution at the base of a stationary crack, J Appl Mech 24 (1957) 109-114

[7] R. Hartranft, G. Sih, The use of eigenfuntions expansions in the general solutions of three-dimensional crack problems, J Math Mech 19 (1969) 123-138

[8] M.R. Ayatollahi, M.J. Pavier, D.J. Smith, Determination of the T-stress from finite element analysis for mode I and mixed mode I/II loading, Int J Fract 91 (1998) 283-298

[9] Personal communication of Z. Knésl and S. Seitl , (2008)